Spectral properties of quasiparticles in silicon: A test of many-body theory

A. S. Kheifets,[1] V. A. Sashin,[1] M. Vos,[1] E. Weigold,[1,*] and F. Aryasetiawan[2]
[1]*Atomic and Molecular Physics Laboratories, Research School of Physical Sciences and Engineering, Australian National University, Canberra, Australian Capital Territory 0200, Australia*
[2]*Research Institute for Computational Sciences, AIST, Tsukuba Central 2, Umezono 1-1-1, Tsukuba Ibaraki 305-8568, Japan*
(Received 22 September 2003; published 22 December 2003)

The spectral function $A(\boldsymbol{q},\omega)$ of silicon has been measured along a number of symmetry directions using high-energy high-resolution electron momentum spectroscopy. It is compared with first-principles calculations based on the interacting one-electron Green's function which is evaluated in the *GW* and the cumulant expansion approximations. Positions of the quasiparticle peaks (dispersion), their widths (lifetimes), and the extensive satellite structures are measured over a broad range of energies and momenta. The band dispersions are well described by both calculations, but the satellite predicted by the *GW* calculation is not observed. Unlike the *GW* calculation, the cumulant expansion calculation gives a significantly better description of the shape and momentum dependence of the satellite structure, presenting a promising approach for studying high-energy excitations.

DOI: 10.1103/PhysRevB.68.233205 PACS number(s): 71.20.Mq, 79.20.Kz, 71.10.−w

The vast majority of experimental and theoretical work on the electronic structure of matter is based on the concept of mean field. Electrons are assumed to interact with a potential (most accurately derived from the density-functional theory) due to the average charge distribution. Theories dealing explicitly with electron-electron correlation are computationally very challenging and few reliable experimental data exist to test the outcome of the calculations. It is therefore very important to provide benchmark tests to validate the many-body calculations and here we show that electron momentum spectroscopy (EMS) of high-quality crystalline targets can provide such tests.

The prototype semiconductor Si has been used as a test bed to study the influence of electronic correlation on the spectral function $A(\boldsymbol{q},\omega)$. Many first-principles calculations have been carried out on bulk silicon, see, e.g., Refs.1–8. The majority of the many-body calculations are based on the *GW* approximation to the interacting one-electron Green's function.[9] Comparison between theory and experiment has, however, been largely limited to analyzing energies of peak positions (band dispersion) and band gaps. Thus angle-resolved photoelectron spectroscopy (ARPES) in combination with tuneable synchrotron light sources has been extensively used to map the dispersion of the bulk bands in silicon along high symmetry directions (see, e.g., Refs. 10–12 and references therein). However, there are very little quantitative data available on the shapes of the quasiparticle peaks (lifetimes), the spectral weights (quasiparticle densities) as a function of momentum, and the satellite density as a function of energy and momentum. These properties of the spectral function arise directly from electron correlation and provide stringent tests for approximations to the full many-body problem. The motivation for testing these theoretical approaches is that first-principles (*ab initio*) calculations of many physical quantities of interest require the interacting one-particle Green's function as an input. It is therefore important to have reliable methods for accurately calculating both the real and imaginary parts of the self-energy, and hence of $A(\boldsymbol{q},\omega)$.

There are severe difficulties in extracting the full $A(\boldsymbol{q},\omega)$ from ARPES experimental data. These difficulties include knowing the specifics of the transitions involved, such as the untangling of final-state effects from the initial-state ones, and the energy and momentum dependence of the matrix elements. In addition, there is usually a significant background count underlying the peak structures, which tends to obscure any continuous satellite contribution. EMS (Refs. 13 and 14) does not have these drawbacks, the cross section (i.e., the measured coincidence count rate) being directly proportional to $A(\boldsymbol{q},\omega)$. Background due to inelastic multiple scattering of the incident and/or emitted electrons can be accurately deconvoluted revealing any satellite contributions.[15]

In the high-energy high-resolution EMS spectrometer, which is fully described elsewhere,[16] a well collimated beam of 50-keV electrons is incident on a thin self-supporting sample. The incident and struck electrons emerge with nearly equal energies (25 keV) and polar angles ($\sim 45°$) relative to the incident (z) direction. The use of such high energies for the incident and emitted electrons reduces greatly the multiple scattering effects, which plagued earlier measurements.[17,18] These high energies have the added advantage that the measurement is relatively bulk sensitive, i.e., it is not strongly affected by surface reconstructions and surface states as is the case for low-energy ARPES measurements. The energies and azimuthal angles of the emitted electrons, detected in coincidence, are measured with electrostatic analyzers fitted with two-dimensional position-sensitive detectors.[16] In high-energy EMS the incoming and outgoing electrons can be accurately treated as plane waves. Knowing their energies E_i and momenta $\boldsymbol{k}_i$, one can infer the binding energy ω and momentum $\boldsymbol{q}$ of the struck electron before the collision through the conservation laws,

$$\omega = E_0 - E_1 - E_2, \quad \boldsymbol{q} = \boldsymbol{k}_1 + \boldsymbol{k}_2 - \boldsymbol{k}_0, \tag{1}$$

where the subscripts $i=0,1,2$ refer to the incident and emitted (scattered and ejected) electrons, respectively.

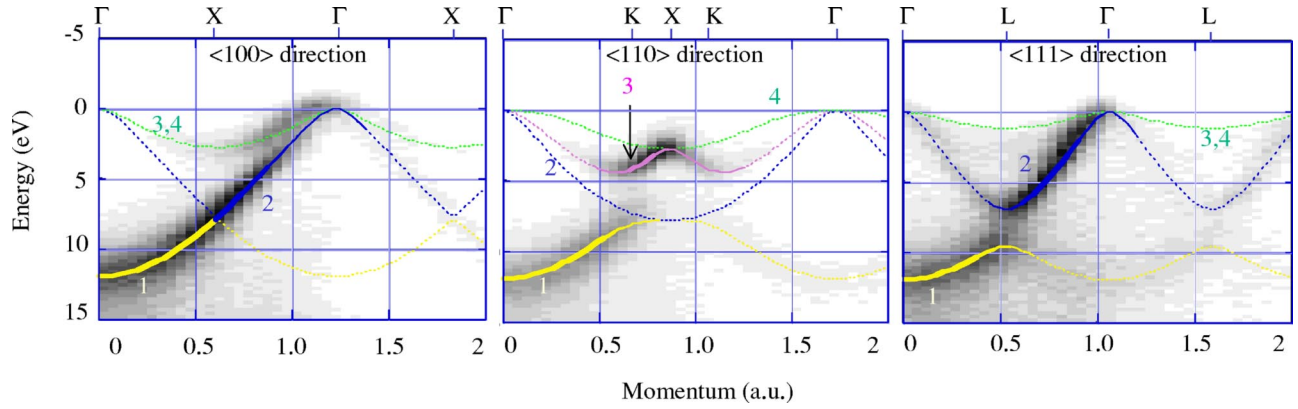

FIG. 1. (Color online) Measured momentum densities along the ⟨100⟩ (left), ⟨110⟩ (middle), and ⟨111⟩ (right) symmetry directions in Si presented in a linear gray scale plot. The calculated LMTO band structure in the repeated zone scheme is superimposed with a line thickness proportional to the momentum density at that momentum value, the dashed sections making no significant contribution.

If the mean scattering plane (horizontal) is defined as the x-z plane, then the momentum component q_y is determined by the relative azimuthal angles ϕ_1, ϕ_2 of the two detected electrons. The momentum components in the x and z directions are determined by the choice of polar angles θ_1, θ_2. In the present case the polar angles were both fixed at 44.3° so that $q_x = q_z = 0$. Different choices of θ_1 and θ_2 about 44.3° give other values for q_x and q_z, in which case the measurements are along lines in momentum space that do not go through $q = 0$ (a Γ point).[16]

In EMS the measurement involves real momenta and it does not depend on the crystal lattice, working as well for (gas-phase) atoms and molecules, amorphous materials as it does for crystals. Hence we can measure the spectral function in any direction. In our setup we can align the sample in such a way that the spectrometer y axis coincides with either the ⟨100⟩, ⟨110⟩, or ⟨111⟩ direction. Diffraction spots of the transmitted beam were observed at a phosphor screen to check the sample alignment. The sample was a thin (~20 nm) silicon crystal with ⟨001⟩ surface normal (see Ref. 17 for sample preparation details). The energy and momentum resolution are, respectively, 1.0 eV and 0.1 a.u. (1 a.u.≈1.89 Å^{-1}).

The measured density plots, up to a binding energy of 15 eV relative to the valence band maximum, are presented in Fig. 1 in a linear gray scale (black being the highest density). Also shown are the bands calculated in the full-potential linear muffin-tin orbital (FP-LMTO) model in the extended zone scheme.[19] Of many momenta which correspond to the same crystal momentum, only a limited number contribute significantly to the Bloch wave. In Fig. 1 the line thickness is proportional to the contribution at that particular momentum to the Bloch wave. At momentum values that do not contribute significantly to the Bloch waves the dispersion is indicated by the dashed lines.

For the measurement along the ⟨100⟩ direction (left panel in Fig. 1), the theory predicts that band 1 in the first Brillouin zone is occupied, as is band 2 to which it changes abruptly at 0.61 a.u. There is no band gap in the dispersion while crossing the first Brillouin zone. After leaving the second Brillouin zone the density drops only gradually to zero. There is in the measurement also an additional branch at smaller binding energy which merges with the main feature at 1.2 a.u. This small contribution comes from Brillouin zone 4, which abuts the ⟨100⟩ direction, and is due to the finite momentum resolution and possibly a small misalignment.

In the ⟨110⟩ symmetry direction (central panel in Fig. 1) the band switches from band 1 to band 3 at the Brillouin crossing, which is with the (111) and $(11\bar{1})$ planes. Here we see the classic band-gap behavior, with band 1 having a minimum in the binding energy at the zone crossing, and diminishing intensity after the crossing. Band 3 on the other hand has zero intensity at zero momentum and its density increases as the momentum increases up to the boundary of the first Brillouin zone, where it has a maximum in the binding energy. The density continues to increase beyond this crossing. It has a minimum in binding energy when it crosses the next set of Brillouin zone boundaries, and its density drops after that when it leaves Brillouin zone 3.

In the ⟨111⟩ direction (right panel of Fig. 1) the density moves from band 1 to band 2 at the boundary of the first

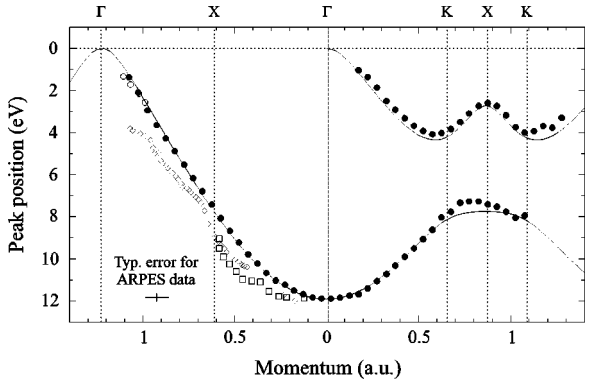

FIG. 2. The experimental dispersion in the peak density (dots) along the ⟨100⟩ (left half) and ⟨110⟩ (right half) directions compared with the LMTO calculation (full line). The open circles are ARPES data taken from Ref. 11 and diamonds and squares are ARPES data taken from Ref. 12.

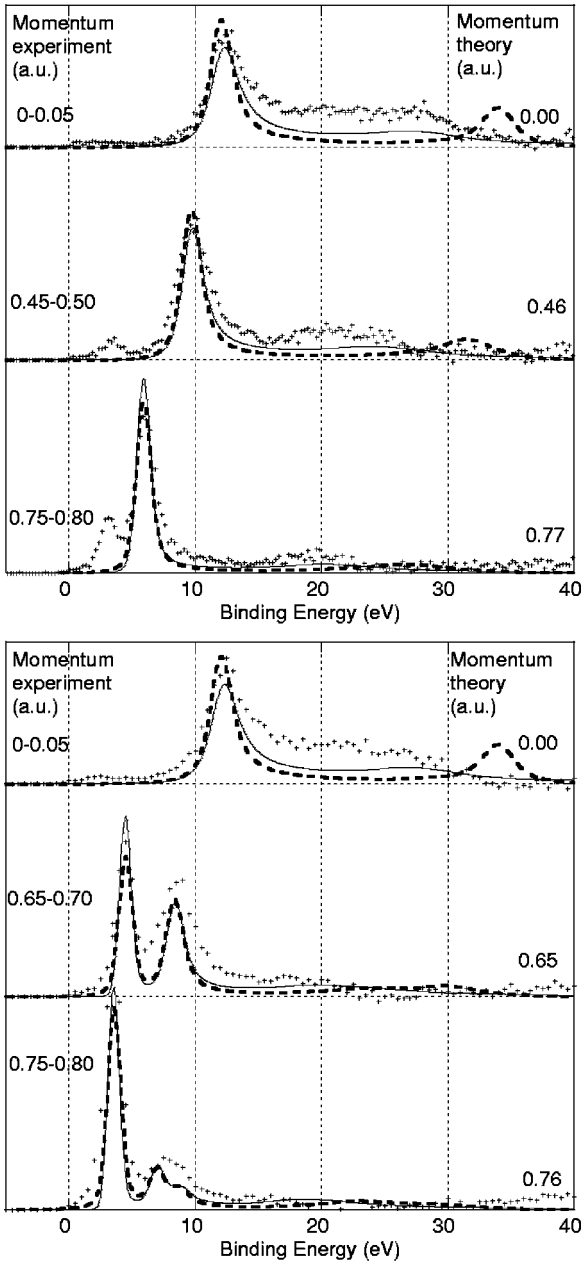

FIG. 3. Spectra at selected momenta along the $\langle 100 \rangle$ (top), $\langle 110 \rangle$ (bottom) directions. The dots are the experimental data deconvoluted for inelastic multiple scattering effects (Ref. 15). The full and dashed lines are the results of the cumulant expansion and *GW* calculations, respectively.

Brillouin zone, band 1 having a minimum in binding energy there and band 2 a maximum. There is again a considerable band gap. In general, the agreement between the measurements and calculations is quite good for all symmetry directions, although it is obvious that the calculated density does not follow exactly the measured density. Leaving aside for the moment the question of the widths in the measured densities, the peak in the observed density in the $\langle 100 \rangle$ direction, for instance, is around $q=0.75$ a.u., whereas for the LMTO calculation it is at the bottom of the band at $q=0$.

A more accurate comparison between the measured and calculated band dispersions is presented in Fig. 2 for the $\langle 100 \rangle$ and $\langle 110 \rangle$ symmetry directions. Here a fitting procedure was used to extract the peak position of the measured density at different momenta and compared with the theory. Also included for the $\langle 100 \rangle$ direction are the ARPES data of Refs. 11 and 12, with typical errors as indicated in the figure. Agreement between the present measurements and the calculations is excellent, the only noticeable deviation is that the observed value of the band gap between bands 1 and 3 in the $\langle 110 \rangle$ direction is smaller than the calculated one. Generally the EMS curves are more smooth and well defined than the ARPES ones. Moreover, all dispersive structures predicted by the theory are reproduced by the experiment.

Returning now to a more detailed discussion of the spectral density distribution, we show in Fig. 3 the spectra at selected momenta along two high-symmetry directions. The experimental spectra at $q=0$ (a Γ point) should be the same and provide a check on the reliability of the data. Also included are the results of two first-principles many-body calculations based, respectively, on the *GW* and the cumulant expansion approximations to the one-electron Green's function.

The theories, convoluted with the experimental energy resolution, are normalized to the experimental data by fitting them to the peak of the quasiparticle structure at the common point $q=0$ (a Γ point), the theories having equal total densities. Both calculations show considerable broadening of the quasiparticle peak, particularly at low momentum. Due to this broadening, which is largest at $q=0$, the peak height there is smaller than at higher q, in agreement with the measurements. In the $\langle 100 \rangle$ direction the small low-binding energy peak arises from the minor contributions from band 4 as discussed earlier.

The observed satellite structure is smooth and continuous up to over 30 eV in binding energy. At zero momentum it accounts for approximately 0.6 of the total spectral weight, its density dropping rapidly with momentum, accounting for around 0.3 of the spectral weight at $q=0.77$ a.u. The *GW* approximation (see also Ref. 1) gives a satellite peak at about 1.5 of the plasmon energy above the main quasiparticle peak. This is not observed in the experiment. The *GW* approximation is known to give accurate quasiparticle energies but the wrong satellite structures. In alkali metals, for example, photoemission spectra show the presence of multiple plasmon satellites whereas the *GW* approximation yields only one at too large an energy.[20]

This shortcoming of the *GW* approximation has been solved by including vertex corrections in the form of the cumulant expansion to the Green's function.[21–23] This takes into account the processes of multiple plasmon creation. As a result the calculated peak positions of the plasmon satellites in alkali metals were found in a much better agreement with the experiment than those predicted by the *GW* scheme itself.[20,24] In the case of silicon (see Fig. 3) the cumulant expansion calculation does not give a distinct satellite peak, instead it gives a broad continuous satellite distribution which drops off smoothly from the main quasiparticle peak. This is in much better agreement with the measurements, as

is the prediction that the satellite density drops off rapidly with increasing q and moves to regions of smaller binding energy.

In conclusion, we have measured the complete spectral function of the prototype semiconductor Si along the three high-symmetry directions. Although the dispersion of the peak in the main quasiparticle structure is well described by the LMTO model, it completely fails to describe the other observed features. Comparison with first-principles calculations shows that the GW approximation predicts the main quasiparticle features quite well, but cannot describe the satellite structure. The cumulant expansion model does rather better, describing the main quasiparticle structures very well. It also gives a reasonable description for the shape and momentum distribution of the satellite density, but significantly underestimates the total satellite contributions at smaller momenta. The agreement is better but not perfect, an encouraging fact as the quantitative comparison between a representation of the many-body wave function and the experimental data should lead to new levels of understanding. Thus, in addition to giving a more accurate description of the quasiparticle dispersion, the EMS data make it pos-sible to directly compare quasiparticle peak shapes, peak in-tensities, and satellite intensity distributions with many-body calculations.

We acknowledge financial support of the Australian Research Council.

*Email address: Erich.Weigold@anu.edu.au

[1] A. Fleszar and W. Hanke, Phys. Rev. B **56**, 10 228 (1997).
[2] A. Kheifets and Y. Cai, J. Phys.: Condens. Matter **7**, 1821 (1995).
[3] W. Borrmann and P. Fulde, Phys. Rev. B **35**, 9569 (1987).
[4] K. Sturm, W. Schülke, and J.R. Schmitz, Phys. Rev. Lett. **68**, 228 (1992).
[5] M.S. Hybertsen and S.G. Louie, Phys. Rev. B **34**, 5390 (1986).
[6] R.W. Godby, M. Schlüter, and L.J. Sham, Phys. Rev. B **37**, 10 159 (1988).
[7] M. Rohlfing, P. Krüger, and J. Pollmann, Phys. Rev. B **48**, 17 791 (1993).
[8] G.E. Engel and W.E. Pickett, Phys. Rev. B **54**, 8420 (1996).
[9] L. Hedin, J. Phys.: Condens. Matter **11**, R489 (1999).
[10] L.S.O. Johansson, P.E.S. Persson, U.O. Karlsson, and R.I.G. Uhrberg, Phys. Rev. B **42**, 8991 (1990).
[11] A.L. Wachs, T. Miller, T.C. Hsieh, A.P. Shapiro, and T.-C. Chiang, Phys. Rev. B **32**, 2326 (1985).
[12] D.H. Rich, G.E. Franklin, F.M. Leibsle, T. Miller, and T.C. Chiang, Phys. Rev. B **40**, 11 804 (1989).
[13] E. Weigold and I.E. McCarthy, *Electron Momentum Spectroscopy* (Kluwer Academic/Plenum, New York, 1999).
[14] M. Vos and I.E. McCarthy, Rev. Mod. Phys. **67**, 713 (1995).
[15] M. Vos, A.S. Kheifets, V.A. Sashin, E. Weigold, M. Usuda, and F. Aryasetiawan, Phys. Rev. B **66**, 155414 (2002).
[16] M. Vos, G.P. Cornish, and E. Weigold, Rev. Sci. Instrum. **71**, 3831 (2000).
[17] S.J. Utteridge, V.A. Sashin, S.A. Canney, M.J. Ford, Z. Fang, D.R. Oliver, M. Vos, and E. Weigold, Appl. Surf. Sci. **162-163**, 359 (2000).
[18] V.A. Sashin, S.A. Canney, M.J. Ford, M.A. Bolorizadeh, D.R. Oliver, and A.S. Kheifets, J. Phys.: Condens. Matter **12**, 125 (2000).
[19] A.S. Kheifets, D.R. Lun, and S.Y. Savrasov, J. Phys. Chem. **11**, 6779 (1999).
[20] F. Aryasetiawan, L. Hedin, and K. Karlsson, Phys. Rev. Lett. **77**, 2268 (1996).
[21] D.C. Langreth, Phys. Rev. B **1**, 471 (1970).
[22] B. Bergersen, F.W. Klus, and C. Blomberg, Can. J. Phys. **51**, 102 (1973).
[23] L. Hedin, Phys. Scr. **21**, 477 (1980).
[24] M. Vos, A.S. Kheifets, E. Weigold, S.A. Canney, B. Holm, F. Aryasetiawan, and K. Karlsson, J. Phys.: Condens. Matter **11**, 3645 (1999).